International Journal of Theoretical Physics, Vol. 30, No. 9, 1991

High-Energy Electron Pair Production on Oxygen

George L. Strobel[1,2] and Robert A. Koss[1,2]

Received October 20, 1989

Electron–positron pair production cross sections are calculated for 50-MeV electrons incident on an oxygen nucleus. The symmetric coplanar cross sections are emphasized. Neglecting exchange, the spectra of forward-scattered projectile electrons is numerically calculated. In the extreme relativistic and nonrelativistic limits for the produced pair kinetic energies, calculated cross sections are similar to those of Bhabha.

1. INTRODUCTION

Recent studies have enhanced interest in calculating lepton pair production cross sections. Pair creation studies in heavy-ion collisions (Kienle, 1986) have revealed correlated electron–positron pairs, emitted back to back with about equal energies. The observations (Cowan *et al.*, 1986) may suggest a resonance exists at 1.83 MeV. Searches in the time-reversed scattering system of electron plus positron have not yet seen such a resonance (Tsertos *et al.*, 1988). Lasers have been proposed (Hora and Loeb, 1986; Kidder, 1974) to initiate the pair production of lepton and antiproton pairs. Lasers would be much more efficient producers of such pairs than are classical particle accelerators. The highest threshold for pair production by lasers is that from vacuum polarization (Hora, 1974).

The experimental production of relativistic positronium has been reported (Alekseev *et al.*, 1984) in observing neutral pion decay. Positronium production cross sections have been estimated for extreme relativistic energies (Bilenkil *et al.*, 1969; Meledin *et al.*, 1971) and calculated to lowest order by Olson (1986) and Holvik and Olsen (1987). The positronium production cross sections are closely related to the (uncorrelated) pair production cross sections. The differences are due to phase space

[1]Institute für Theoretische Physik, University of Tübigen, D 7400 Germany.
[2]Permanent address: Physics Department, University of Georgia, Athens, Georgia 30602-9986.

0020-7748/91/0900-1235$06.50/0

and normalization factors. The positronium production process has the electron and positron produced in a bound state, while in pair production, the produced electron and positron are free. High-energy electron pair production in the field of a nucleus is similar to electromagnetic pair production in the field of a nucleus (Bethe and Heitler, 1934). The lowest order quantum electrodynamic (QED) description of electron-induced pair production uses Feynman diagrams analogous to the electromagnetic pair production Feynman diagrams. Several authors (Bethe and Maximon, 1954; Davies *et al.*, 1954; Olsen *et al.*, 1975; Landro *et al.*, 1987) have calculated the differential cross section for electromagnetic lepton pair production in the Coulomb field with arbitrary Z.

Lepton pair production is also an important energy loss mechanism for high-energy electrons traversing the atmosphere. We therefore consider 50-MeV electrons incident on an oxygen nucleus that forward scatter and lose no more than 10 MeV of energy in the rest frame of the target nucleus. Bhabha (1935) calculated electron-induced pair production using a Weizacker–Williams impact parameter calculation, treating the electron as traveling straight ahead. Bhabha calculated approximate expressions for the differential cross sections when the produced lepton pair shared only a small amount of kinetic energy, and also when the kinetic energy shared by the produced pair was large compared to the electron mass. Here a cross section is calculated that in addition interpolates between those extremes. The final-state electron will be considered as moving straight ahead after the pair production.

In lowest order QED, for electron-induced pair production on a spinless point nucleus of charge Z, there are seven Feynman diagrams, plus seven exchange diagrams contributing to the reaction amplitude. In the region of phase space considered, the exchange diagrams are neglected and we associate the higher-energy final-state electron with the projectile. We also neglect diagrams where both photons interact with the target nucleus. These are small and would vanish in the limit of no recoil energy for the final-state nucleus.

The Feynman diagrams included in a lowest order QED expansion of the amplitude are shown in Figure 1. On the right-hand side of Figure 1 are shown the no-nuclear-recoil limit of the same diagrams. The last three diagrams vanish in this limit. For 50-MeV electrons forward, or nearly forward scattered from an oxygen target nucleus, the recoil energy is small compared to the electron mass. Therefore, these diagrams are neglected in the calculations reported here. The positron four-momentum is denoted by P_3 in this calculation, and the projectile four-momentum in the final state is denoted by P_1. Z denotes the nuclear charge and the electron mass is m. Conservation of four-momenta between the initial and final states is

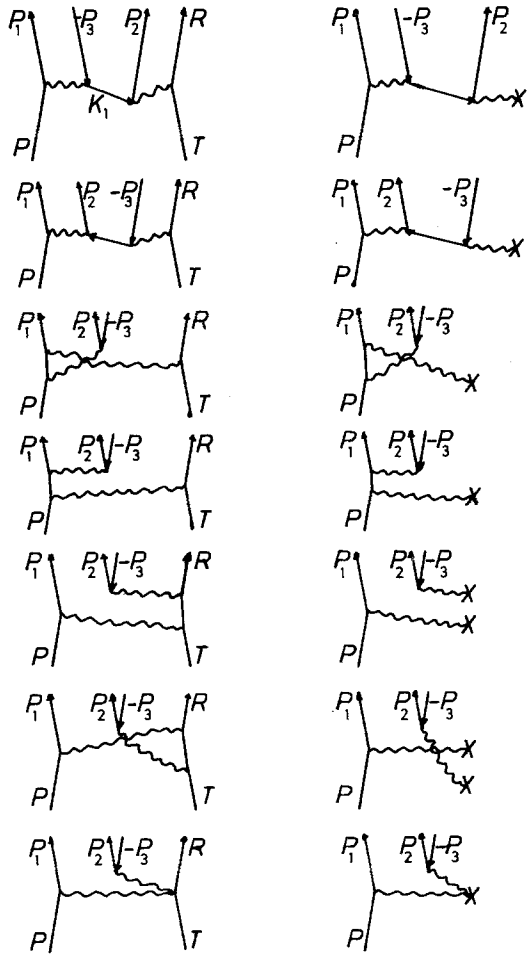

Fig. 1. Lowest order QED Feynman diagrams for pair production by an electron incident on a target nucleus with initial four-momenta P and T, respectively. The final positron momentum is P. The right half shows the no-recoil-energy-approximation diagrams for pair production. The last three diagrams vanish.

indicated by the relation

$$P+T=P_1+P_2+P_3+R$$

where the initial state is an electron of four-momentum P incident onto a nucleus of four-momentum T. In the final state, the produced electron has four-momentum P_2, and the recoiling nucleus has four-momentum R.

2. THEORY

The invariant amplitude (Bjorken and Drell, 1964) is written as

$$M = C \sum_{i=1}^{4} M_i \tag{1}$$

where

$$M_i = N_i / D_i \tag{2}$$

and where C is a common coefficient defined as

$$C = -ie^4 Z / 2m \tag{3}$$

and the D_i are defined in Table I. The denominators D_i come from the pair of photon propagators and also the fermion propagator associated with each of the first four diagrams of Figure 1 that are included in this calculation. The rest of the invariant amplitude is written as a product of two factors,

$$\begin{aligned} N_1 &= F_1 G_1 \\ N_2 &= F_2 G_2 \\ N_3 &= F_3 G_3 \\ N_4 &= F_4 G_4 \end{aligned} \tag{4}$$

These F and G factors can be determined from the Feynman diagrams of Figure 1. The amplitudes F and G are exhibited in Table I.

The completely polarized cross section is proportional to $|M|^2$. To calculate the unpolarized cross section, the initial- and final-state spins are at

Table I

$D_1 = (P-P_1)^2(T-R)^2(K_1^2-m^2)$	$K_1 = P-P_1-P_3$
$D_2 = (P-P_1)^2(T-R)^2(K_2^2-m^2)$	$K_2 = P_1+P_2-P$
$D_3 = (P-K_3)^2(T-R)^2(K_3^2-m^2)$	$K_3 = P-P_2-P_3$
$D_4 = (P_2+P_3)^2(T-R)^2(K_4^2-m^2)$	$K_4 = P_1+P_2+P_3$
$S = T+R$	
$F_1 = \bar{U}(P_1)(4P\!\!\!/ - 2P\!\!\!/_1)U(P)$	
$F_2 = F_1$	
$F_3 = \bar{U}(P_1)S\!\!\!/(K\!\!\!/_3+m)U(P)$	
$F_4 = \bar{U}(P_1)(K\!\!\!/_4+m)S\!\!\!/U(P)$	
$G_1 = \bar{U}(P_2)S\!\!\!/(K\!\!\!/_1+m)V(P_3)$	
$G_2 = \bar{U}(P_2)(K\!\!\!/_2+m)S\!\!\!/V(P_3)$	
$G_3 = \bar{U}(P_2)(-4P\!\!\!/_3-2P\!\!\!/_2)V(P_3)$	
$G_4 = G_3$	

first summed over. Thus, one arrives at the four diagonal and six off-diagonal traces,

$$\sum_{\text{spins}} |M|^2 = C^2 \sum_{ij}^{4} \text{Tr}\, F_i \bar{F}_j \,\text{Tr}\, G_i G_j / D_i D_j \tag{5}$$

The values of these traces are indicated in the Appendix.

One should average over the initial-state spin components, and sum over the final-state spin components, rather than summing over each. Accounting for initial-state averaging is done by including a factor of 1/2. There are two identical electrons in the final state, even though exchange is neglected here. So the statistical factor is $S=2$. The factors appear as the first two factors in the denominator of equation (6) below.

The most differential cross section is 12-fold differential and includes a four-dimensional delta function conserving momenta and energy between the initial and final states. This cross section is trivially integrated over the three-momentum of the recoil nucleus, which is not observed. Also, here, the differential cross section is integrated over the magnitude of the positron momenta, eliminating the four-dimensional delta function conserving four-momenta between the initial and final states. Writing $e^2 = 4\pi\alpha$, where α is the fine structure constant $\cong 1/137$, the eightfold differential cross section remaining is written as

$$\frac{d\sigma}{dq_1\, dq_2\, d\Omega_1\, d\Omega_2\, d\Omega_3} = \frac{16m^2\alpha^4 Z^2 (197.3)^2 q_1^2 q_2^2 \sum_{\text{spins}} |\sum_{i=1}^{4} M_i|^2 q_3}{2 \cdot 2(4\pi)^4 v\omega A \omega_1 \omega_2 \{\omega_R + \omega_3 + q_e y \omega_3 / q_3\}} \tag{6}$$

The ω, ω_1, ω_2, ω_3, and ω_r are the energies of the projectile, the final electron, the pair-produced electron and positron, and of the recoil nucleus, respectively. The last factor in the denominator of equation (6) comes from the energy-conserving delta function when the magnitude of the positron momentum was integrated over. The units are fermi** 2/MeV**2 Sr**3 for the cross section. The electron mass m is in MeV, the target nucleus mass A is also in MeV. The projectile momentum is q, in MeV/c, the final electron momenta are q_1 for the projectile, q_2 for the pair-produced electron, and q_3 for the positron. M_i is from the invariant amplitude squared, summed over spins; see equation (1). The frame where the target nucleus is at rest is chosen to work in so that v is the velocity of the projectile electron, about 1 in our units of c, the speed of light. $\mathbf{q}$, $\mathbf{q}_1$, $\mathbf{q}_2$, $\mathbf{q}_3$ are the three-momenta of the projectile, final-state electron, pair-produced electron, and positron in the final state, respectively. y is the cosine of the angle between the positron

momentum and the difference between the initial and the final electron momenta, that is,

$$y = \mathbf{q}_3 \cdot \mathbf{q}_e / q_3 q_e, \qquad \mathbf{q}_3 = \mathbf{q} - \mathbf{q}_1 - \mathbf{q}_2 \tag{7}$$

The projectile-electron final three-momentum $\mathbf{q}_1$ is considered to be unscattered. Thus, when the azimuthal angles ϕ_2 and ϕ_3 for the pair-produced electron and positron differ by π, a coplanar final state geometry results. When the spherical polar angles of the three-momenta of the produced pair, θ_2 and θ_3, are equal, the calculated cross section is referred to as a symmetric coplanar cross section. It is this cross section that is primarily reported in the next section.

3. RESULTS

In Figure 2, the calculated forward symmetric coplanar cross section is shown. The produced pair share about 1 MeV of kinetic energy. The geometry shown is for the projectile to be unscattered, and for the produced pair to also be traveling in the forward direction. Thus, for the curve shown in Figure 2, all three final-state leptons are traveling with colinear three-momenta. This forward spectrum peaks for a positron momentum of about 0.8 MeV/c. The general shape of the spectrum can be understood from final-state phase-space considerations visible in equation (5). When this curve is integrated over all positron momentum values, one obtains about 1700 f^2/

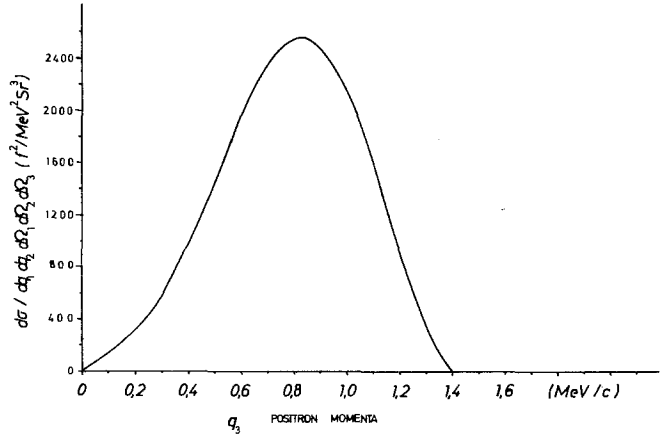

Fig. 2. Forward positron spectrum for 50-MeV electrons losing 2 MeV energy on oxygen. All final-state leptons go straight ahead.

MeV Sr[3], which value appears in Figure 3. Figure 3 shows the symmetric coplanar energy loss cross section versus the production angle for the pair. The projectile has 50 MeV energy and the final state electron has 48 MeV energy. Thus, the electron has undergone a 2-MeV energy loss, but is unscattered in direction. This symmetric coplanar cross section is peaked for pair production also in the forward direction. As the pair is produced at larger angles with respect to the projectile direction, the cross section monotonically decreases with angle for a projectile energy loss of 2 MeV.

As the energy loss of the projectile approaches about 1.4 MeV or less, this pair production cross section becomes isotropic in a smooth fashion. In this small energy loss region, the integrated-over-angle pair-production cross section, for a given projectile energy loss, is proportional to the cube of the kinetic energy that the produced pair share, in agreement with Bhabha. When the projectile energy loss exceeds about 1.4 MeV, the energy shared by the produced pair is no longer small compared to the electron rest mass, and the calculation of Bhabha is not valid in this phase space region. When the produced pair share about 0.8 MeV kinetic energy, as in Figure 3, the cross section is not isotropic. Instead the symmetric pair production cross section can be characterized as having a cone angle of 1/gamma. Here, gamma is something like m/E, where E is an average energy of the leptons of the produced pair. At any rate, the calculated symmetric pair production cross section is forward peaked, and for an energy loss of 2 MeV for the projectile, falls to half its maximum value when the cone angle of the produced pair is about 0.2 rad.

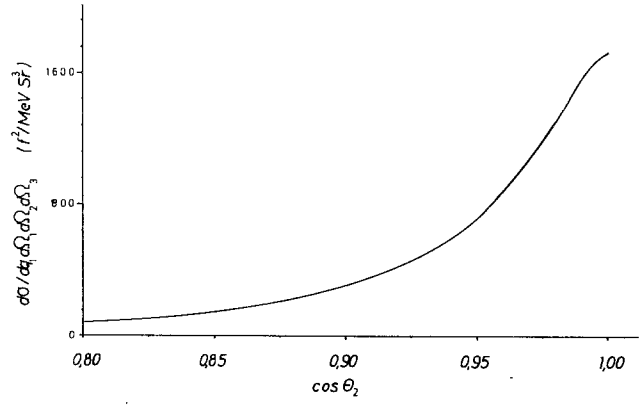

Fig. 3. Symmetric coplanar cross section for pair production for 50-MeV electrons losing 2 MeV on oxygen. These conditions nearly match those at the peak seen in Figure 8.

Figure 4 shows the symmetric coplanar cross section for pair production where the final electron energy is held to various constant values. As the produced pair share less kinetic energy, the symmetric coplanar cross section becomes more nearly isotropic. Conversely, as the projectile loses more energy, the cross section becomes more strongly peaked in the forward direction. In Figure 4, this cross section is shown on a logarithmic scale. One observes that the differential cross section at forward angles

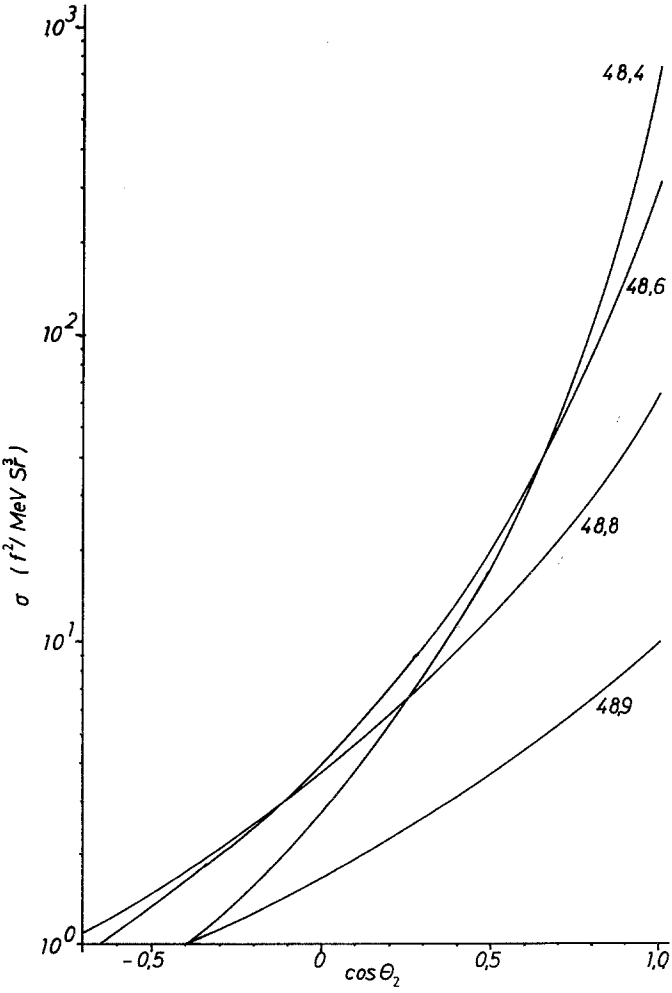

Fig. 4. Symmetric coplanar cross section for various small energy losses by projectile electron versus scattering angle of the produced pair. Note the logarithmic scale.

rises as the energy loss increases. The half-width of the calculated differential symmetric coplanar cross section decreases as the energy loss of the projectile increases.

Figure 5 shows the symmetric coplanar cross section for projectile energy losses of 1.8 MeV and more, versus the cone angle of the produced pair. The cross section is still forward peaked and the slope of the cross section continues to rise as the projectile energy loss increases. The peak cross section continues to increase with the projectile energy loss, but a new feature occurs. As the projectile loses more than 2 MeV, the pair production

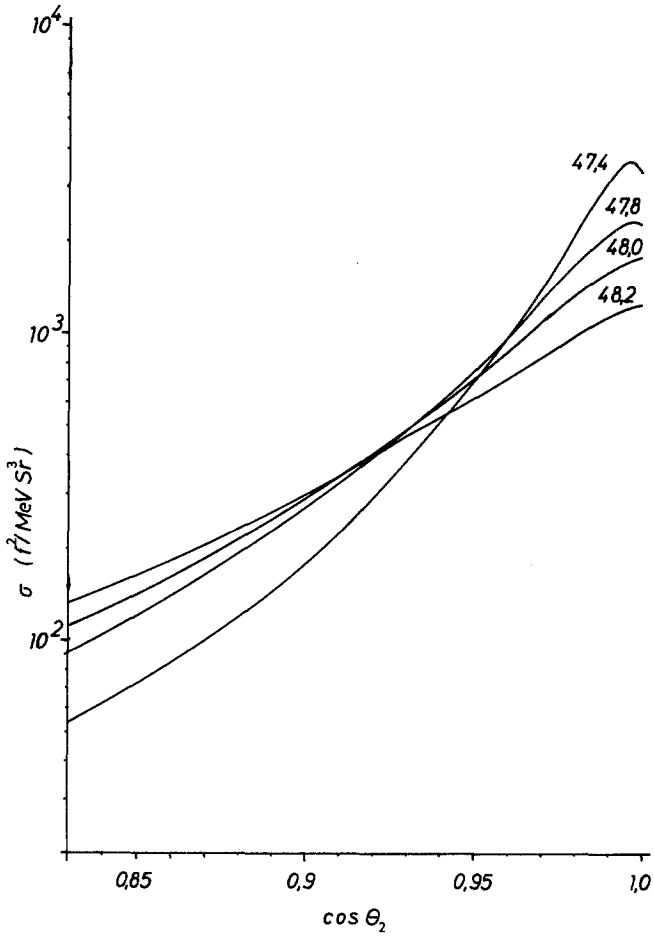

Fig. 5. Symmetric coplanar pair production for projectile energy losses near the peak of Figure 8 versus scattering angle of the produced pair. The produced pair share a kinetic energy roughly equal to their rest mass.

cross section becomes peaked at small angles, but not at the exact forward direction. The peak cross section occurs when the pair is produced at a small cone angle slightly different than zero.

Figure 6 shows the symmetric coplanar cross sections calculated for energy losses of 3 and 4 MeV. The peak cross section continues to increase with projectile energy loss, and the calculated cross sections fall almost exponentially with the cosine of the pair production angle. Figure 7 shows the coplanar cross sections for projectile energy losses of 5 and 10 MeV. For these cases, the energy shared by the produced pair is becoming large compared to the electron rest mass. The calculated symmetric coplanar cross section is strongly forward peaked, and falls off nearly exponentially with

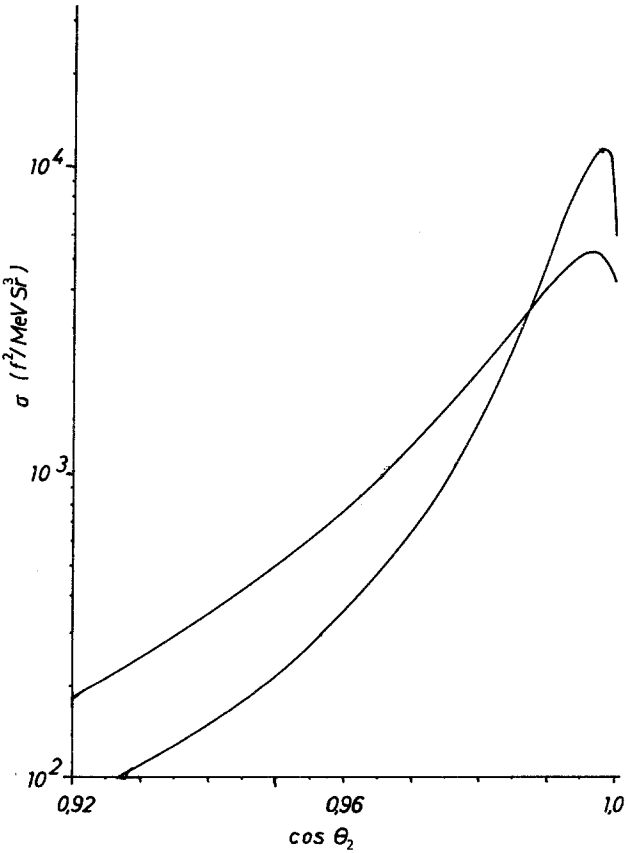

Fig. 6. Symmetric coplanar pair production cross sections versus pair production scattering angle. Note a near exponential falloff. The produced pair share a kinetic energy larger than their rest masses.

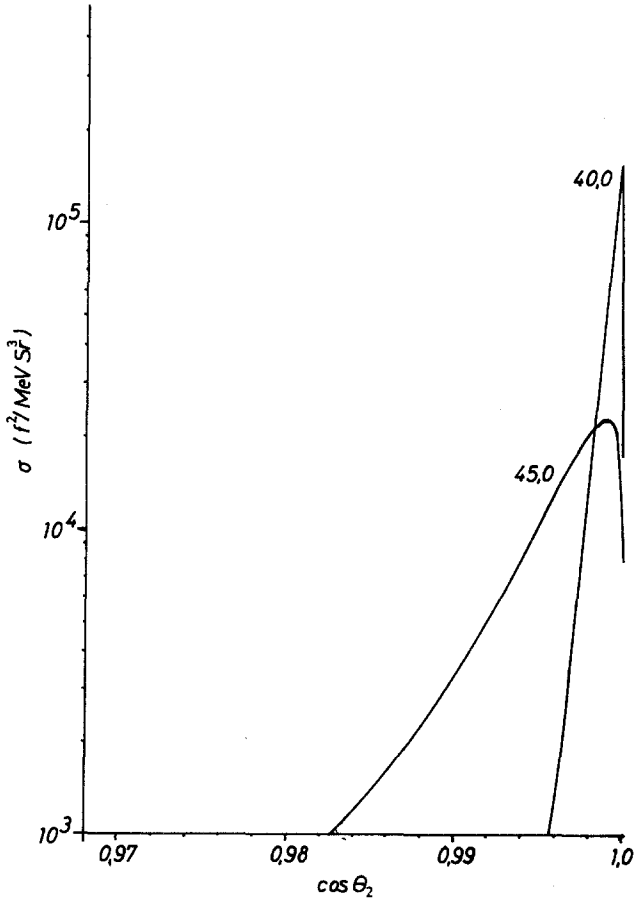

Fig. 7. Symmetric coplanar pair production cross section versus pair scattering angle. Note the limited range of angle shown, and near exponential falloff of cross section from the peak values. The produced pair share a kinetic energy large compared to their rest masses.

the pair production angle. For these cases, numerically integrating over all final-state geometries produces a differential cross section similar in energy dependence to the result of Bhabha, when the rest energy of the pair is negligible in comparison to the kinetic energy shared.

When the energy loss of the projectile becomes comparable to the projectile energy initially, exchange diagrams are expected to contribute noticeably to the pair production amplitude. The numerically integrated cross section shown in Figure 8 is stopped at a minimum final electron energy of 40 MeV, for which the produced electron would have a maximum energy of about 9 MeV. For projectile energy losses greater than this, the exchange

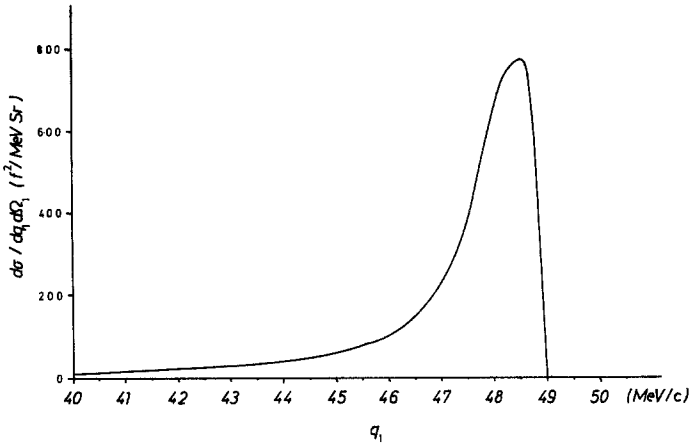

Fig. 8. Inclusive calculated forward electron cross section versus final electron momentum. The projectile was forward scattered. The production angles of the produced pair are numerically integrated over.

contributions become comparable to the direct diagrams in the lowest order QED amplitude. The direct-only numerically-integrated cross section (not shown) continues smoothly to zero as the energy loss approaches the initial energy.

APPENDIX

The traces of various matrices needed in equation (5) are assembled below. The F and G are defined in Table I. Each P, S, and K is a four-vector momentum. $S = T + R$ is the sum of the target plus recoil nucleus four-momenta. After summing over all initial and final state spins, one obtains the following traces:

$$F_1\bar{F}_1 = 4(m^2 + P \cdot P_1), \qquad G_4\bar{G}_4 = 4(P_2 \cdot P_3 - m^2)$$

$$F_1\bar{F}_3 = 2[m(P_1 \cdot S + S \cdot K_3 + P \cdot S) + P \cdot K_3P_1 \cdot S - P \cdot SP_1K_3 + P \cdot P_1S \cdot K_3]/m$$

$$F_1\bar{F}_4 = 2[m(P_1 \cdot S + S \cdot K_4 + P \cdot S) + P \cdot SP \cdot K_4 - P \cdot K_4P_1 \cdot S + P \cdot P_1S \cdot K_4]/m$$

$$
\begin{aligned}
F_3\bar{F}_4 &= S^2(m^2 + P\cdot K_3 - K_3\cdot K_4 - P\cdot K_4 - P_1\cdot K_3 - P\cdot P_1 + P_1\cdot K_4)\\
&\quad + 2S\cdot K_3 S\cdot K_4 + 2S\cdot PS\cdot K_4 + 2S\cdot K_3 P_1\cdot S + P\cdot SP_1\cdot S\\
&\quad + [S^2 P\cdot K_3 P_1\cdot K_4 - 2S\cdot K_3 P\cdot K_4 P_1\cdot S + 2S\cdot K_3 P\cdot P_1 S\cdot K_4\\
&\quad + (2P\cdot SP_1\cdot S - P\cdot P_1 S^2)K_3\cdot K_4\\
&\quad - P_1\cdot K_3(2P\cdot SS\cdot K_4 - P\cdot K_4 S^2)]/m^2\\
F_3\bar{F}_3 &= S^2(2P\cdot K_3 - 2P_1\cdot K_3 + K_3^2 - P\cdot P_1 + m^2)\\
&\quad + 2P_1\cdot SP\cdot S + 4P_1\cdot SK_3\cdot S\\
&\quad + [(4P\cdot K_3 S\cdot K_3 - 2P\cdot SK_3^2)(P_1\cdot S)\\
&\quad - 2P_1\cdot K_3 P\cdot K_3 S^2 + P\cdot P_1 S^2 K_3^2]/m^2\\
F_4\bar{F}_4 &= 2S^2 P_1\cdot K_4 + S^2 K_4^2 + 4P\cdot SK_4\cdot S\\
&\quad - 2S^2 P\cdot K_4 + 2P\cdot SP_1\cdot S - P\cdot P_1 S^2 + S^2 m^2\\
&\quad + [(P\cdot S)(4K_4\cdot P_1 S\cdot K_4 - 2K_4^2 P_1\cdot S)\\
&\quad - 2P\cdot K_4 P_1\cdot K_1 S^2 + P\cdot P_1 S^2 K_4^2]/m^2\\
G_1\bar{G}_4 &= 2[m(P_3\cdot S - K_1\cdot S - P_2\cdot S)\\
&\quad + (K_1\cdot SP_2\cdot P_3 - S\cdot P_3 K_1\cdot P_2 + P_2\cdot SK_1\cdot P_3)/m]\\
G_2\bar{G}_4 &= 2[m(P_3\cdot S - P_2\cdot S - K_2\cdot S)\\
&\quad + (K_2\cdot SP_2\cdot P_3 - K_2\cdot P_3 P_2\cdot S + K_2\cdot P_2 S\cdot P_3)/m]\\
G_1\bar{G}_2 &= S^2(K_1\cdot K_2 - K_2\cdot P_2 - P_3\cdot K_2 - P_2\cdot P_3\\
&\quad + K_1\cdot P_2 + K_1\cdot P_3 - m^2)\\
&\quad + 2(S\cdot P_3 S\cdot K_2 - S\cdot K_1 S\cdot K_2\\
&\quad + S\cdot P_3 S\cdot P_2 - S\cdot K_1 S\cdot P_2)\\
&\quad + (K_1\cdot P_3 K_2\cdot P_2 S^2 - 2K_1\cdot SP_3\cdot K_2 P_2\cdot S\\
&\quad + 2K_1\cdot SP_2\cdot P_3 K_2\cdot S\\
&\quad + 2K_1\cdot K_2 P_3\cdot SP_2\cdot S - K_1\cdot K_2 P_2\cdot P_3 S^2\\
&\quad - 2K_1\cdot P_2 P_3\cdot SK_2\cdot S + K_1\cdot P_2 P_3\cdot K_2 S^2)/m^2\\
G_2\bar{G}_2 &= 4S\cdot P_3 S\cdot K_2 + 2S\cdot P_2 S\cdot P_3\\
&\quad - S^2(2P_2\cdot K_2 + K_2^2 + 2K_2\cdot P_3 + P_2\cdot P_3 + m^2)\\
&\quad + [P_2\cdot P_3 K_2^2 S^2 - 2P_2\cdot SP_3\cdot SK_2^2\\
&\quad + 2P_2\cdot K_2(2S\cdot P_3 S\cdot K_2 - S^2 P_3\cdot K_2)]/m^2
\end{aligned}
$$

$$G_1\bar{G}_1 = S^2(2K_1 \cdot P_3 - K_1^2 - P_2 \cdot P_3 + 2K_1 \cdot P_2 - m^2)$$
$$+ 2P_2 \cdot SP_3 \cdot S - 4K_1 \cdot SP_2 \cdot S$$
$$+ [2P_3 \cdot K_1(2P_2 \cdot SK_1 \cdot S - P_2 \cdot K_1 S^2)$$
$$- 2P_3 \cdot SP_2 \cdot SK_1^2 + P_2 \cdot P_3 S^2 K_1^2]/m^2$$

REFERENCES

Alekseev, G. D., *et al.* (1984). *Yadernaya Fizika*, **40**, 139 (*Soviet Journal of Nuclear Physics* **40**, 8).

Bethe, H. A., and Heitler, W. (1934). *Proceedings of the Royal Society of London A*, **146**, 83.

Bethe, H. A., and Maximom, L. C. (1954). *Physical Review*, **93**, 768.

Bhabha, H. J. (1935). *Proceedings of the Royal Society*, **152A**, 559.

Bilenkil, S. M., Nguyan van Hieu, Nemenove, L. L., and Tkebuchava, F. G. (1969). *Yadernaya Fizika*, **10**, 812 (*Soviet Journal of Nuclear Physics*, **1970**, 469).

Bjorken, J. D., and Drell, S. D. (1964). *Relativistic Quantum Mechanics*, McGraw-Hill, New York, Appendix B.

Cowan, T., *et al.* (1986). *Physical Review Letters*, **56**, 444.

Davies, H., Bethe, H. A., and Maximom, L. C. (1954). *Physical Review*, **93**, 788.

Holvik, E., and Olsen, J. A. (1987). *Physical Review*, **35D**, 2124.

Hora, H. (1974). In *Laser Interaction and Related Plasma Phenomena*, H. Schwarz, and H. Hora, eds., Plenum Press, New York, Vol. 3B, p. 819.

Hora, H., and Loeb, H. W. (1986). *Zeitschrift für Flugwissenschaften*, **10**, 393.

Kidder, R. (1974). In *Laser Interaction and Related Plasma Phenomena*, H. Schwarz, and H. Hora, eds. Plenum Press, New York, p. 889.

Kienle, P. (1986). *Annual Reviews of Nuclear Science*, **36**, 605.

Landro, M., Mork, K. S., and Olsen, H. A. (1987). *Physical Review*, **6D**, 44.

Meledin, G. V., Serbo, V. G., and Slivkov, A. K. (1971). *Pis'ma Zhurnal Eksperimental'noi i Teoreticheskoi Fizika*, **13**, 98 [*JETP Letters*, **13**, 68 (1971)].

Olsen, H. A. (1986). *Physical Review D*, **33**, 2033.

Olsen, H. A., Maximom, L. C., and Wergeland, H. (1975). *Physical Review*, **106**, 27.

Tsertos, H., *et al.* (1988). *Physics Letters*, **207**, 273.